Supporting Information: Improving the Energy Efficiency of CO_2 Conversion in Non-equilibrium Plasmas Through Pulsing

Vincent Vermeiren and Annemie Bogaerts*

Department of Chemistry, Research group PLASMANT, University of Antwerp, Universiteitsplein 1, 2610 Antwerp, Belgium

E-mail: annemie.bogaerts@uantwerpen.be

1 List of Chemical Reactions Included in the Model

Table S1: Electron impact reactions calculated with cross sections, using the calculated EEDF, as explained in section 2.3 of the main paper, as well as the references where the data are adopted from.

No.	Reaction	Ref	Note*
(X1)[a]	$e^- + CO_2 \rightarrow 2e^- + CO_2^+$	S1	
(X2)[b]	$e^- + CO_2 \rightarrow 2e^- + O + CO^+$	S1	
(X3)[b]	$e^- + CO_2 \rightarrow O^- + CO$	S1	
(X4)[b]	$e^- + CO_2 \rightarrow e^- + O + CO$	S1	
(X5)[a]	$e^- + CO_2 \rightarrow e^- + CO_2[e_1]$	S1	
(X6)[c]	$e^- + CO_2 \leftrightarrow e^- + CO[v_i]$	S1	i=a,b,c,d
(X7)[c]	$e^- + CO_2[v_i] \leftrightarrow e^- + CO_2[v_j]$	S1	i,j=0-21
(X8)[b]	$e^- + CO \rightarrow 2e^- + CO^+$	S2	
(X9)[b]	$e^- + CO \rightarrow C + O^-$	S3	
(X9bis)[b]	$e^- + CO \rightarrow e^- + C + O$	S4	
(X10)[a]	$e^- + CO \rightarrow e^- + CO[e_x]$	S4	x=1-4
(X11)[c]	$e^- + CO \rightarrow e^- + CO[v_i]$	S4	i=1-10
(X12)[b]	$e^- + O_2 \rightarrow e^- + O + O$	S5	
(X12M)[a]	$e^- + O_2 + M \rightarrow e^- + O_2^- + M$	S5	
(X13)[b]	$e^- + O_2 \rightarrow O + O^-$	S5	
(X14)[c]	$e^- + O_2 \leftrightarrow e^- + O_2[v_i]$	S5	i=1,2,3
(X15)[a]	$e^- + O_2 \leftrightarrow e^- + O_2[e_x]$	S5	x=1,2

a) Same cross section also used for $CO_2 v_i$ (i = the various vibrationally excited levels)
b) Cross section also used for $CO_2 v_i$, modified by lowering the energy threshold by the energy of the excited state of $CO_2 v_i$
c) Cross section for the various levels (i,j) scaled and shifted using Fridman's approximation from the $(0 \rightarrow 1)$ cross-section
* v_0 is ground state

Table S2: Electron impact reactions using analytical expressions for the rate coefficients, given in m^3/s and m^6/s, for two-body and three-body reactions, respectively, as well as the references where the data are adopted from. T_g and T_e are given in K and eV, respectively.

No.	Reaction	Rate coefficient	Reference
(E1a)	$e^- + CO_2^+ \rightarrow CO(v_1) + O$	$1 \times 10^{-11} T_e^{-0.5} T_g^{-1}$	S6,S7
(E1b)	$e^- + CO_2^+ \rightarrow C + O_2$	$1 \times 10^{-11} T_e^{-0.5} T_g^{-1}$	S8
(E2)[a]	$e^- + CO_4^+ \rightarrow CO_2 + O_2$	$1.61 \times 10^{-13} T_e^{-0.5}$	S8
(E3)	$e^- + CO^+ \rightarrow C + O$	$3.46 \times 10^{-14} T_e^{-0.48}$	S9,S10
(E4)[a]	$e^- + O + M \rightarrow O^- + M$	1×10^{-43}	S7

[a] The primary source was not accessible

Table S3: Ion-ion and ion-neutral reactions, as well as the references where the data are adopted from. The rate coefficients are given in m^3/s and m^6/s, for two-body and three-body reactions, respectively. T_g is given in K.

No.	Reaction	Rate coefficient	Reference
(I1)	$CO_2 + CO^+ \rightarrow CO_2^+ + CO$	1.0×10^{-15}	S11,S12
(I2a)[b]	$CO_2 + O^- + CO_2 \rightarrow CO_3^- + CO_2$	1.5×10^{-40}	S11,S13
(I2b)[b]	$CO_2 + O^- + CO \rightarrow CO_3^- + CO$	1.5×10^{-40}	S11,S13
(I2c)	$CO_2 + O^- + O_2 \rightarrow CO_3^- + O_2$	3.1×10^{-40}	S11,S13
(I3)	$CO_2 + O_2^- + M \rightarrow CO_4^- + M$	4.7×10^{-41}	S11,S13
(I4)	$CO + O^- \rightarrow CO_2 + e$	5.5×10^{-16}	S11,S14
(I5)	$CO + CO_3^- \rightarrow 2CO_2 + e$	5×10^{-19}	S15
(I6)[a]	$CO_3^- + CO_2^+ \rightarrow 2CO_2 v_b + O$	5×10^{-13}	S7
(I7)[a]	$CO_4^- + CO_2^+ \rightarrow 2CO_2 v_b + O_2$	5×10^{-13}	S7
(I8)[a]	$O_2^- + CO_2^+ \rightarrow CO_2 v_1 + O_2 + O$	6×10^{-13}	S7
(I9)	$CO_3^- + O \rightarrow CO_2 + O_2^-$	8×10^{-17}	S16
(I10a)[a]	$CO_4^- + O \rightarrow CO_3^- + O_2$	1.12×10^{-16}	S11
(I10b)[a]	$CO_4^- + O \rightarrow CO_2 + O_2 + O^-$	1.4×10^{-17}	S11
(I11)	$O + O^- \rightarrow O_2 + e$	2.3×10^{-16}	S17
(I12)[a]	$O + O_2^- \rightarrow O_2 + O^-$	1.5×10^{-16}	S11
(I13)	$O_2^- + M \rightarrow O_2 + M + e$	$2.7 \times 10^{-16} (\frac{T_g}{300})^{0.5} exp(-5590/T_g)$	S18,S19
(I14)[c]	$O^- + M \rightarrow O + M + e$	$2.3 \times 10^{-15} exp(-26000/T_g)$	S19–S21

[a] The primary source was not accessible

[b] The rate coefficient of $CO_2 + O^- + He \rightarrow CO_3^- + He$ was used, due to the lack of further information.

[c] For usual values of gas temperature, i.e. $T_g \ll 26000$ K, the rate coefficient is very low, as pointed out by Gudmundsson.[S22]

Table S4: Neutral-neutral reactions, as well as the references where the data are adopted from. The rate coefficients are given in m^3/s and m^6/s, for two-body and three-body reactions, respectively. T_g is given in K. The α parameter determines the effectiveness of lowering the activation energy for reactions involving vibrationally excited levels of the molecules (see details in S23,S24).

No.	Reaction	Rate coefficient	α	References
(N1)	$CO_2 + M \rightarrow CO + O + M$	$6.06 \times 10^{-16} exp(-52525/T_g)$	0.82	S25
(N2)	$CO_2 + O \rightarrow CO + O_2$	$2.8 \times 10^{-17} exp(-16400/T_g)$	0.57	S26
(N3)	$CO_2 + C \rightarrow 2CO$	$< 10^{-21}$	n.a.	S27
(N4)[a]	$CO + O + M \rightarrow CO_2 + M$	$8.3 \times 10^{-46} exp(-1510/T_g)$	0.0	S28,S29
(N5)	$O_2 + CO \rightarrow CO_2 + O$	$4.2 \times 10^{-18} exp(-24000/T_g)$	0.5	S29
(N6)	$O_2 + C \rightarrow CO + O$	$1.99 \times 10^{-16} exp(-2010/T_g)$	0.0	S30
(N7)	$O + C + M \rightarrow CO + M$	$2.14 \times 10^{-41} (\frac{T_g}{300})^{-3.08} exp(-2144/T_g)$	n.a.	S29,S31
(N8)	$O + O + M \rightarrow O_2 + M$	$5.2 \times 10^{-47} exp(900/T_g)$	n.a.	S29,S31
(N9)	$O_2 + M \rightarrow O + O + M$	$3.0 \times 10^{-12} \frac{1}{T_g} exp(-59380/T_g)$	0.0	S29,S31

[a] Multiply by 7, 3 or 12 for M= CO_2, CO or O_2 respectively.

Table S5: Neutral reactions between vibrationally excited molecules, as well as the references where the data are adopted from. The rate coefficients are given in m^3/s and m^6/s, for two-body and three-body reactions, respectively. T_g is given in K.

No.	Reaction	Rate coefficient	References
(V1)	$CO_2 v_a + M \rightarrow CO_2 + M$	$7.14 \times 10^{-15}\, exp(-177\, T_g^{-1/3} + 451\, T_g^{-2/3})$	S32–S34
(V2a)	$CO_2 v_1 + M \rightarrow CO_2 v_a + M$	$4.25 \times 10^{-7}\, exp(-407\, T_g^{-1/3} + 824\, T_g^{-2/3})$	S34–S36
(V2b)	$CO_2 v_1 + M \rightarrow CO_2 v_b + M$	$8.57 \times 10^{-7}\, exp(-404\, T_g^{-1/3} + 1096\, T_g^{-2/3})$	S34–S36
(V2c)	$CO_2 v_1 + M \rightarrow CO_2 v_c + M$	$1.43 \times 10^{-7}\, exp(-252\, T_g^{-1/3} + 685\, T_g^{-2/3})$	S34–S36
(V3)	$CO v_1 + M \rightarrow CO + M$	$1.0 \times 10^{-18}\, T_g\, exp(-150.7\, T_g^{-1/3})$	S37
(V4)	$O_2 v_1 + M \rightarrow O_2 + M$	$1.3 \times 10^{-14}\, exp(-158.7\, T_g^{-1/3})$	S33,S34
(V5)	$CO_2 v_1 + CO_2 \rightarrow CO_2 v_a + CO_2 v_b$	$1.06 \times 10^{-11}\, exp(-242\, T_g^{-1/3} + 633\, T_g^{-2/3})$	S34–S36
(V6)	$CO_2 v_1 + CO_2 \rightarrow CO_2 + CO_2 v_1$	$1.32 \times 10^{-18}\, (\frac{T_g}{300})^{0.5} \frac{250}{T_g}$	S38,S39
(V7)	$CO v_1 + CO \rightarrow CO + CO v_1$	$3.4 \times 10^{-16} (\frac{T_g}{300})^{0.5}\, (1.64 \times 10^{-6}\, T_g + \frac{1.61}{T_g})$	S40,S41
(V8)	$CO_2 v_1 + CO \rightarrow CO_2 + CO v_1$	$4.8 \times 10^{-12}\, exp(-153\, T_g^{-1/3})$	S34,S35

2 Average Temperature Gains and Losses by Plasma Pulsing

Figure 5 in the main paper shows the total vibrational and gas temperature gains and losses between the pulses for different plasma pulse and interpulse times. Here we show the temperature gains and losses, averaged over all pulses, for exactly the same plasma pulse and interpulse times. This gives additional information about the actual temperature values. It is clear that the average gas temperature losses rise with increasing interpulse time.

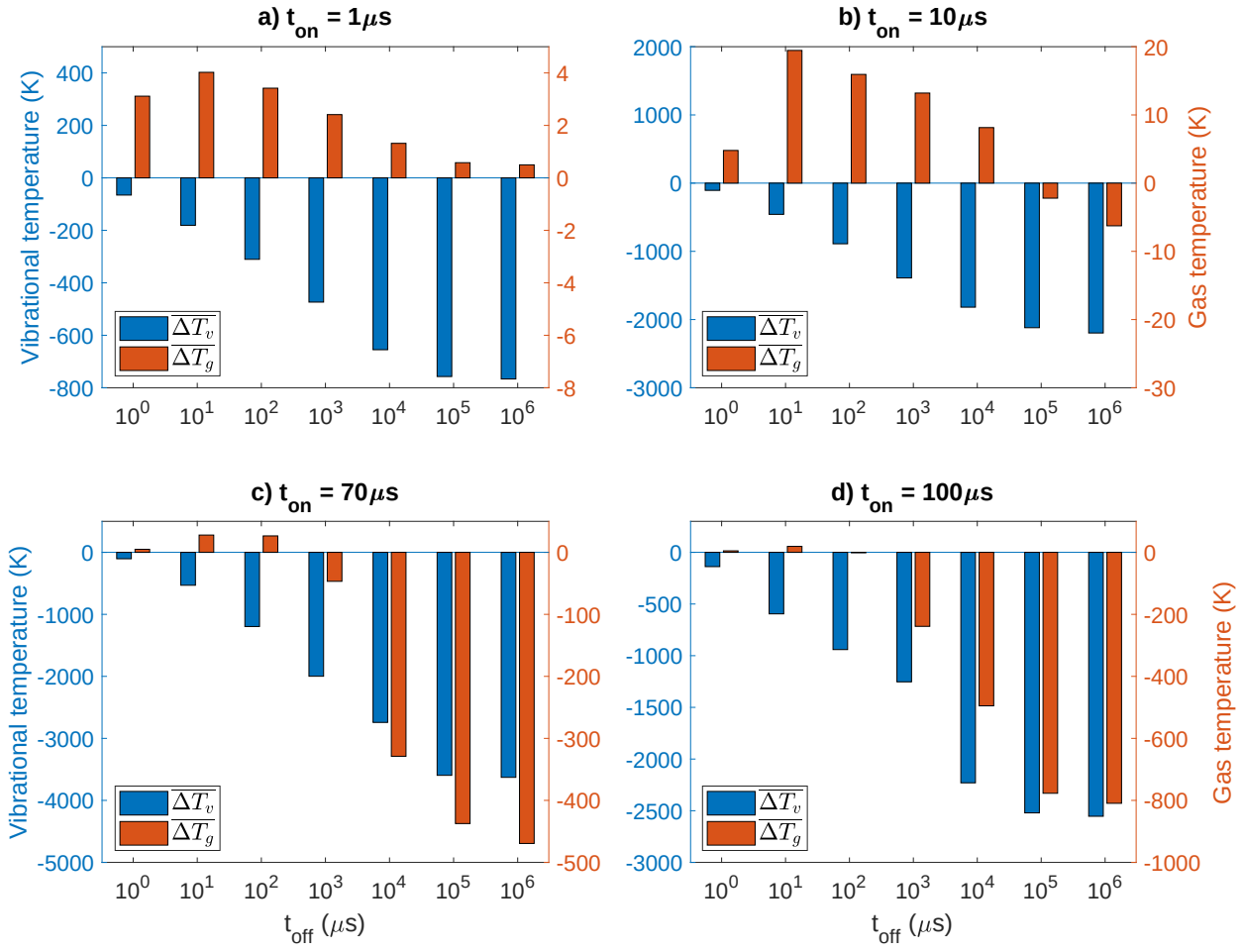

Figure S1: Average vibrational and gas temperature gains and losses between the pulses, for different plasma pulse and interpulse times.

3 Temporal Evolution of the Gas Temperature

In figure S2, we show the evolution of the gas temperature from the initial time t_0 until the plasma end time t_{end} (when the total fixed SEI of 1 eV/molec is reached), for four different plasma pulse times (t_{on} = 1, 10, 70, and 100 μs)and five different interpulse times (t_{off} = 10 μs, 100 μs, 1 ms, 10 ms, 1 s). For comparison, we also plot the gas temperature evolution for the continuous plasma with the same SEI. The x-axis represents the time from the start of the first pulse to the end of the last pulse. However, because the total time is different for different plasma pulse and interpulse times, to reach the same SEI, the reader should not compare different points on the x-axis, since they can represent different total times.

For all of the plasma pulse times, a longer interpulse time yields a lower maximum gas temperature, since there is more cooling. Moreover, the maximum gas temperature is lower than in the continuous plasma for all plasma pulse and interpulse times. At t_{off} = 1 s, the gas temperature completely drops to room temperature. With increasing plasma pulse times, it can be seen that the gas maximum for a given interpulse time increases.

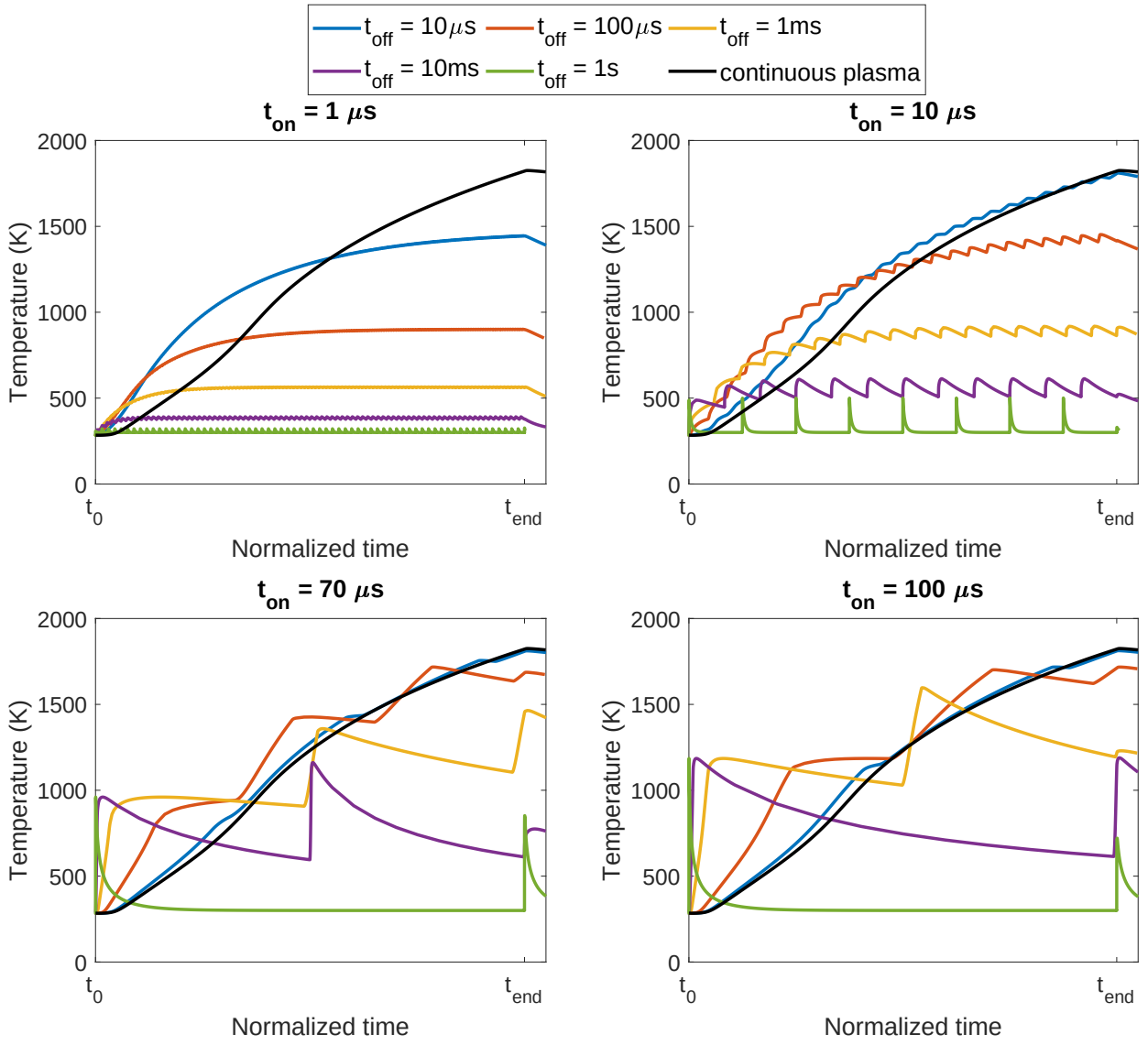

Figure S2: Time-evolution of the gas temperature between the start of the first pulse and the end of the last pulse, for different plasma pulse times and interpulse times. t_{end} is defined by the time when the total fixed SEI of 1 eV/molec is reached. For comparison, the gas temperature in the continuous plasma, for the same SEI, is also plotted (black curves).

4 Average Vibrational and Gas Temperature During the Pulses

Figure S3 illustrates the average vibrational and gas temperature during the pulses (i.e., averaged over all plasma pulse times), for different plasma pulse and interpulse times, as well as the corresponding values in the continuous plasma, for comparison. For short plasma pulse

times, the vibrational temperature is always lower than in the continuous plasma. Indeed, the pulses are too short to reach a maximum vibrational temperature. For longer plasma pulse times, the vibrational temperature becomes higher than in the continuous plasma at interpulse times above 1 ms, because of the enhanced cooling, causing less VT relaxation. In all cases, the average gas temperature is comparable to a continuous plasma for short interpulse times (below 1 ms), and drops with increasing interpulse time. This is consistent with figure S2. Note that while for both $t_{on} = 70$ μs and $t_{on} = 100$ μs, the average vibrational temperature at $t_{off} = 10$ ms lies above the continuous plasma, these pulse conditions do not show an increased energy efficiency. Indeed, while the vibrational-translational non-equilibrium is enhanced by the plasma cooling, leading to a higher vibrational temperature, the enhancement is not sufficient to create a fast overpopulation of the vibrational levels (as seen in figure 8 of the main paper, and figure S5 below).

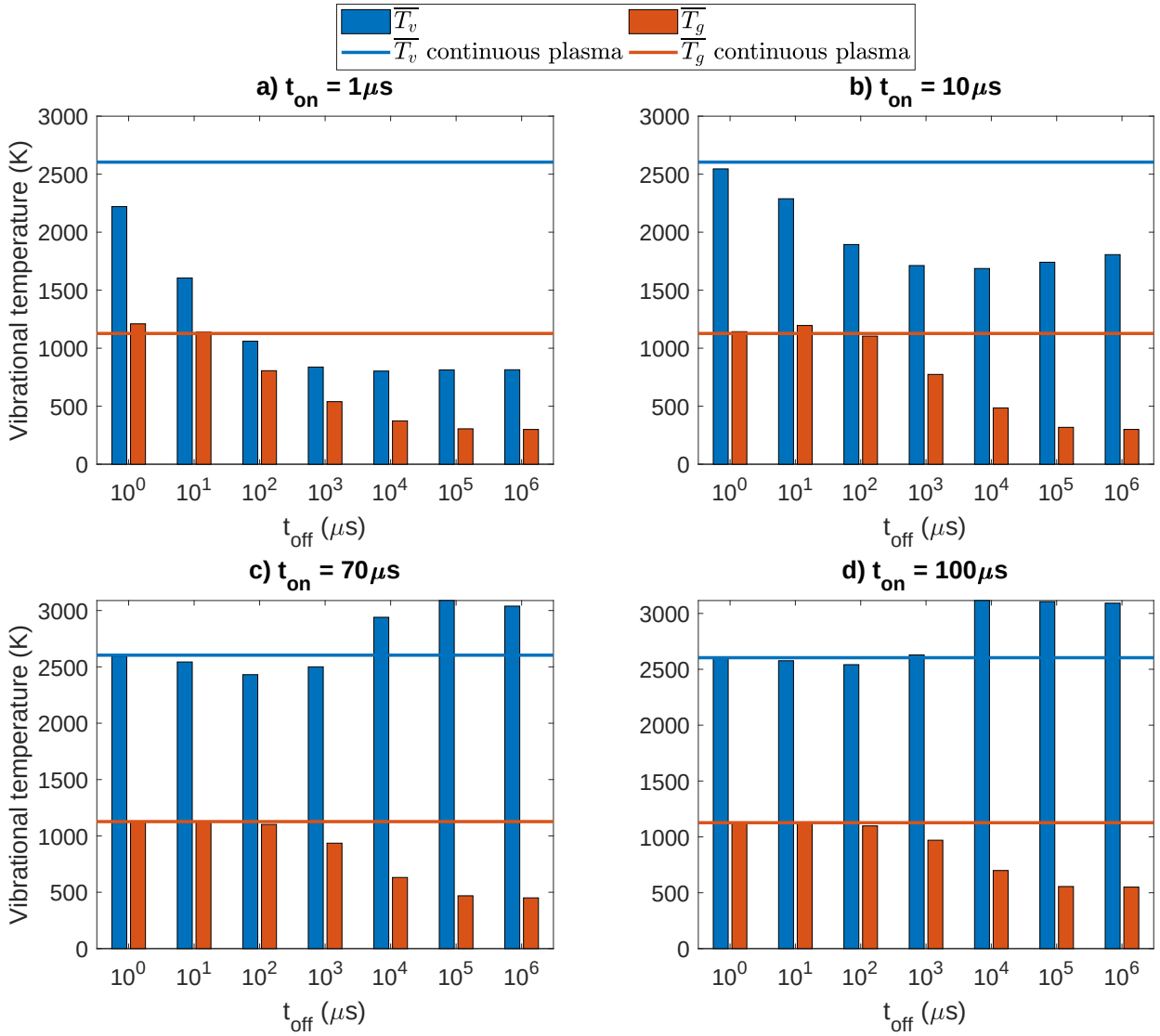

Figure S3: Average vibrational and gas temperature in the plasma pulses for different plasma pulse and interpulse times. The horizontal lines correspond to the continuous plasma.

5 VDF Halfway the Plasma

Figure S4 illustrates the VDFs halfway of the plasma, i.e., when half of the SEI (thus 0.5 eV/molec) is deposited. For $t_{on} = 70$ μs and $t_{on} = 100$ μs, this happens in the first pulse, so we only show the VDFs for shorter plasma pulses, i.e., $t_{on} = 1$ μs and $t_{on} = 10$ μs. We also compare with the VDF in the continuous plasma, and with the Boltzmann plots at the corresponding gas temperatures. For $t_{on} = 1$ μs (panel a), the VDFs are always lower than in the continuous plasma, and they are most populated for short interpulse times, when there

is limited time for relaxation. At longer interpulse times, the VDF completely relaxes in between the pulses, and the pulse time is too short to reach significant overpopulation of the vibrational levels. At $t_{on} = 10$ μs, the VDF coincides with the continuous plasma at short interpulse times, but it is depleted for longer interpulse times. However, due to the low gas temperature at $t_{off} = 1$ s, the characteristic time scales of the VV relaxation is low, while that of the VT relaxation is high, resulting again in a fast and pronounced overpopulation of the higher vibrational levels, so the VDF becomes again very similar to that of a continuous plasma.

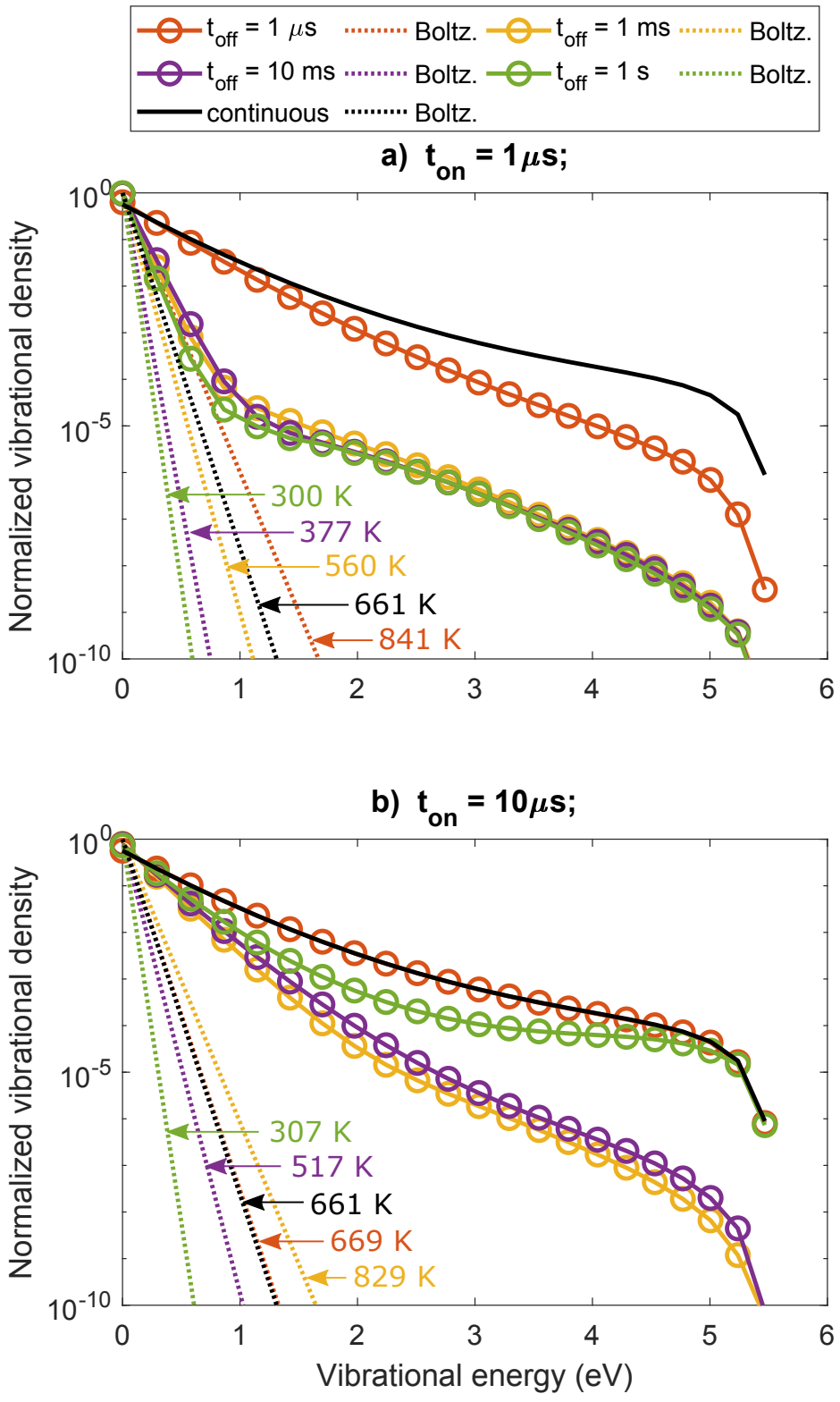

Figure S4: VDFs halfway the plasma, i.e., when half of the SEI is deposited (0.5 eV/molec), for $t_{on} = 1$ μs (a, top panel), and for $t_{on} = 10$ μs (b, bottom panel), and for four different interpulse times. The VDF in the continuous plasma is also plotted (black curve), as well as the Boltzmann plots for each case at the corresponding gas temperatures.

6 VDF at the End of the Plasma

In figure S5, we plot the VDFs at the end of the plasma, for t_{on} = 10 μs and t_{on} = 100 μs. They should be compared with the VDFs for t_{on} = 1 and 70 μs, plotted in figure 9 of the main paper.

For t_{on} = 10 μs and t_{on} = 100 μs, the VDFs at the end of the plasma, for different interpulse times look very similar to the VDFs for 70 μs. The VDF at the end of the plasma coincides with the one of the continuous plasma for short interpulse times (1 μs to 1 ms), but it reaches a higher population for longer interpulse times, similar to t_{on} = 70 μs (see figure 9 of the main paper). However, while both plasma pulse time show a large overpopulation of the VDF at t_{off} = 1 s, the energy efficiency with respect to t_{on} = 70 μs remains lower. Indeed, for t_{on} = 10 μs, the short plasma pulse time enhances the vibrational temperature loss due to pulsing (see figure 6 in the main paper). Also, while the overpopulation at the end of the pulse is high, the overpopulation does not last long enough for vibrational induced dissociation. For t_{on}=100 μs, there are two pulses to reach the SEI of 1 eV/molec at t_{off} = 1 s. However, during a significant portion of the first pulse, the VDF was thermalized, so our model predicts lower energy efficiencies for these conditions than for t_{on} = 70 μs (see figure 1 in the main paper).

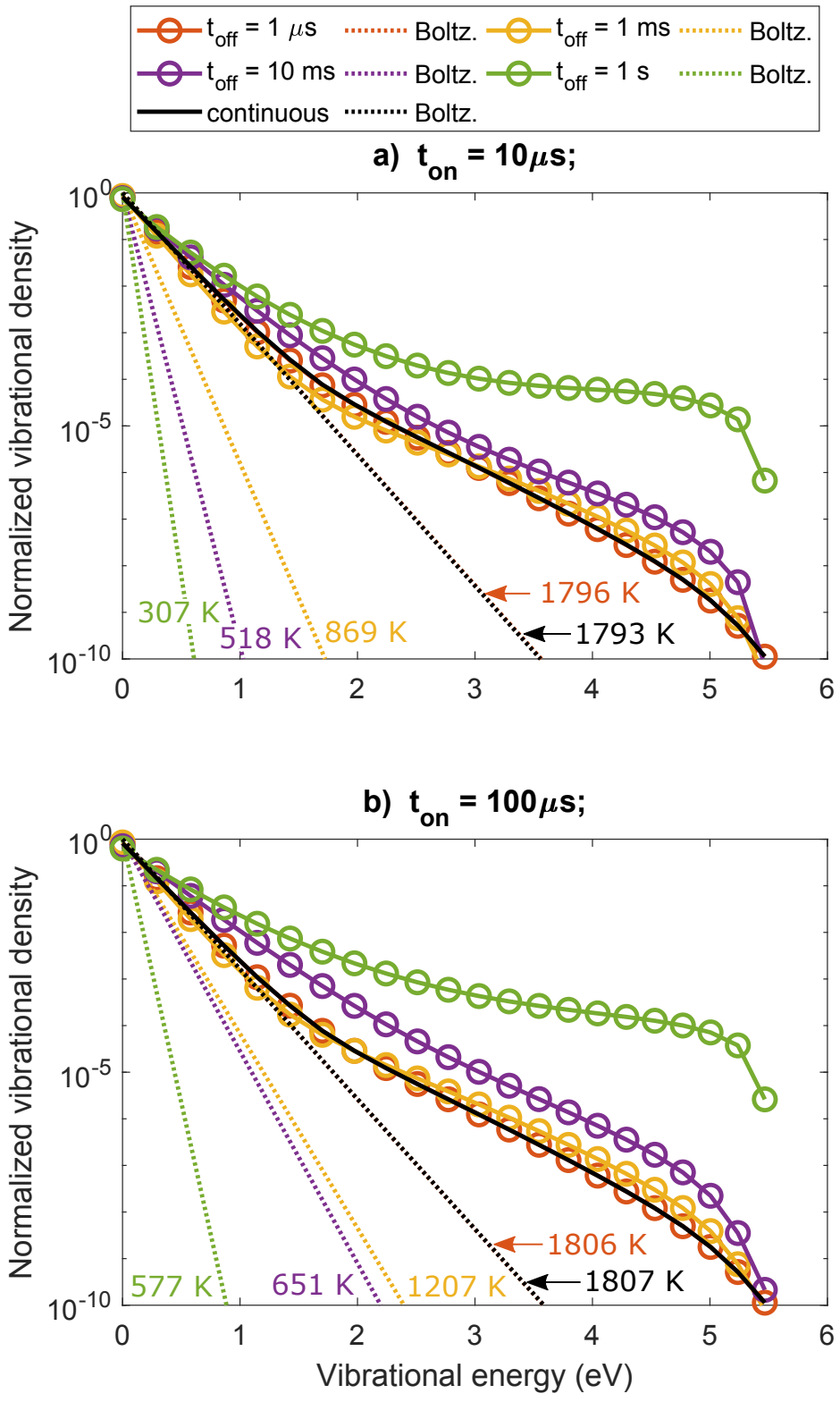

Figure S5: VDFs at the end of the plasma, for $t_{on} = 1$ μs (a, top panel), and $t_{on} = 100$ μs (b, bottom panel) for four different interpulse times. The VDF in the continuous plasma is also plotted (black curve), as well as the Boltzmann plots for each case at the corresponding gas temperatures.

7 Time-evolution of the Vibrational and Gas Temperature in a Continuous Plasma for Different Ionization Degrees and Reduced Electric Fields

Figures S6-S8 show the time-evolution of the vibrational and gas temperature in a continuous plasma, for different ionization degrees, and for reduced electric fields of 50 Td, 100 Td and 150 Td, respectively. The end time is different in each case, as it is defined by the time when the total fixed SEI of 1 eV/molec is reached. At low ionization degrees, the vibrational temperature reaches a maximum value early in time, but this maximum shifts to later times upon higher ionization degree. This is correlated with the lower characteristic time scale of electron impact vibrational excitation with higher ionization degree, as was shown in figure 2 of the main paper. At an ionization degree of 5×10^{-6} and higher, the maximum value is reached close to or at the end of the plasma (i.e., when the SEI of 1 eV/molec is reached). For these conditions, pulsing will not increase the energy efficiency, because the loss of vibrational energy between the pulses will not be compensated by a higher vibrational temperature. This is true for a reduced electric field of 50 and 100 Td (figures S6 and S7). At 150 Td, this is already the case for an ionization degree of 5×10^{-7} (figure S8).

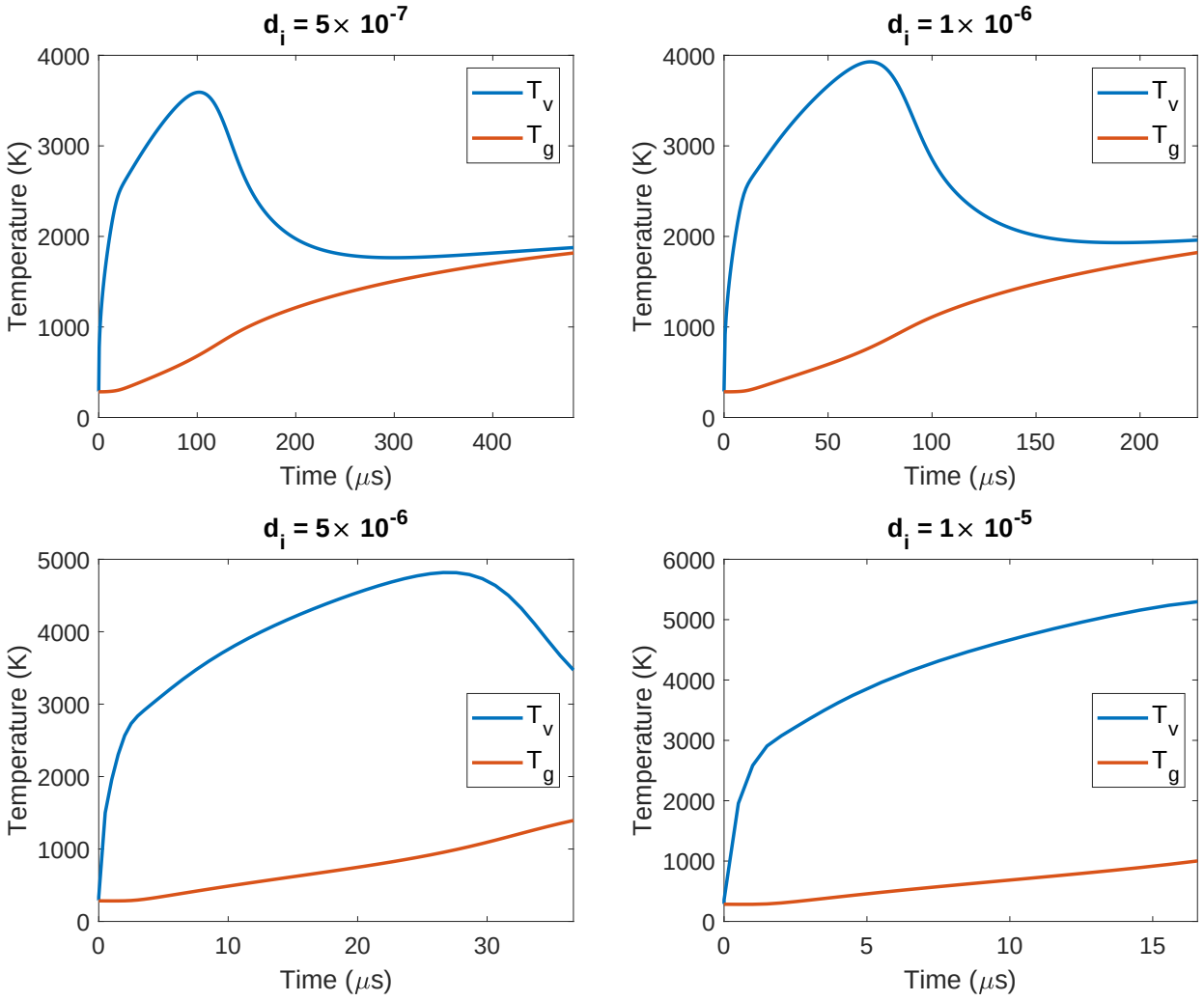

Figure S6: Time-evolution of the vibrational and gas temperature in a continuous plasma for different ionization degrees, and a reduced electric field of 50 Td.

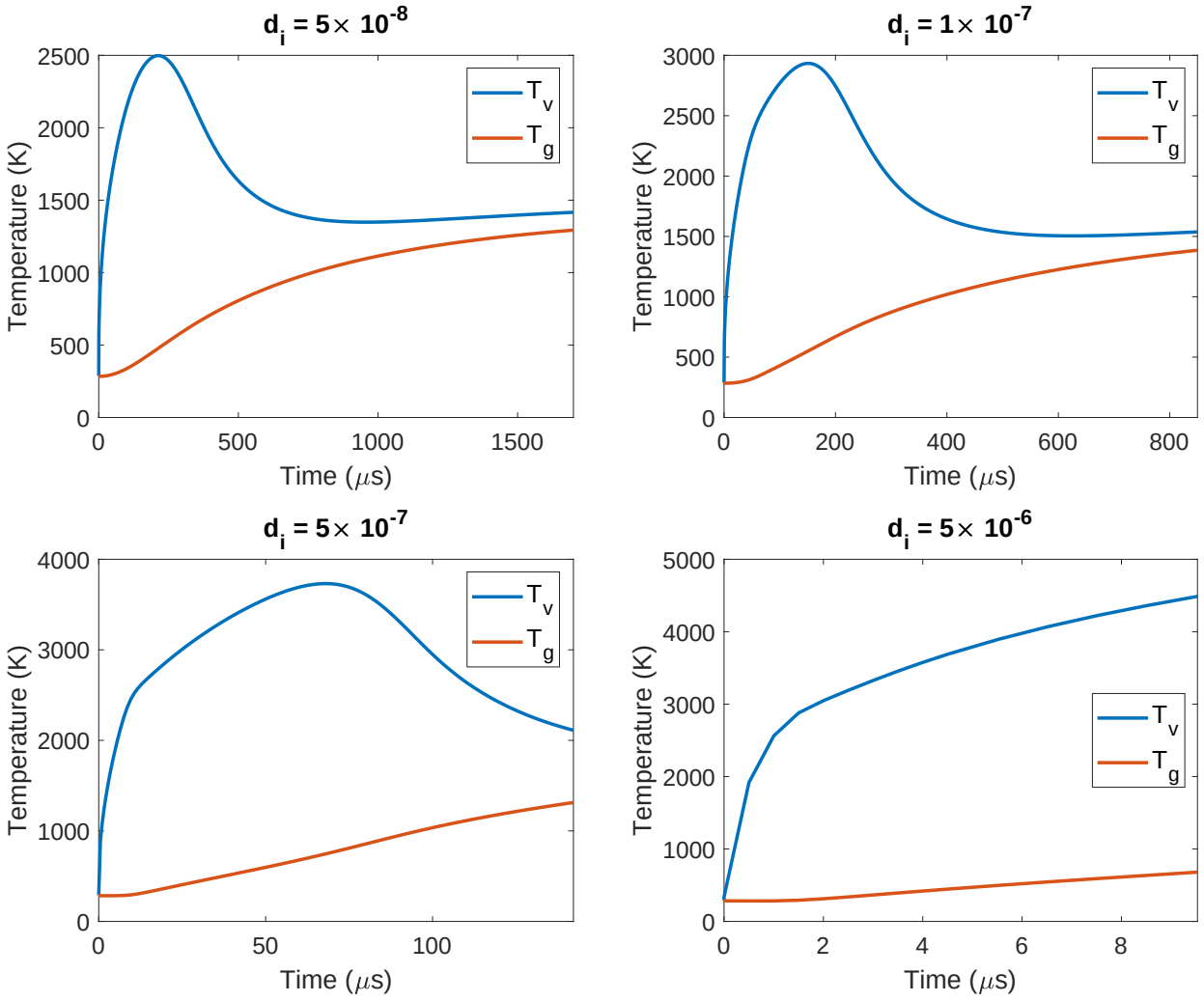

Figure S7: Time-evolution of the vibrational and gas temperature in a continuous plasma for different ionization degrees, and a reduced electric field of 100 Td.

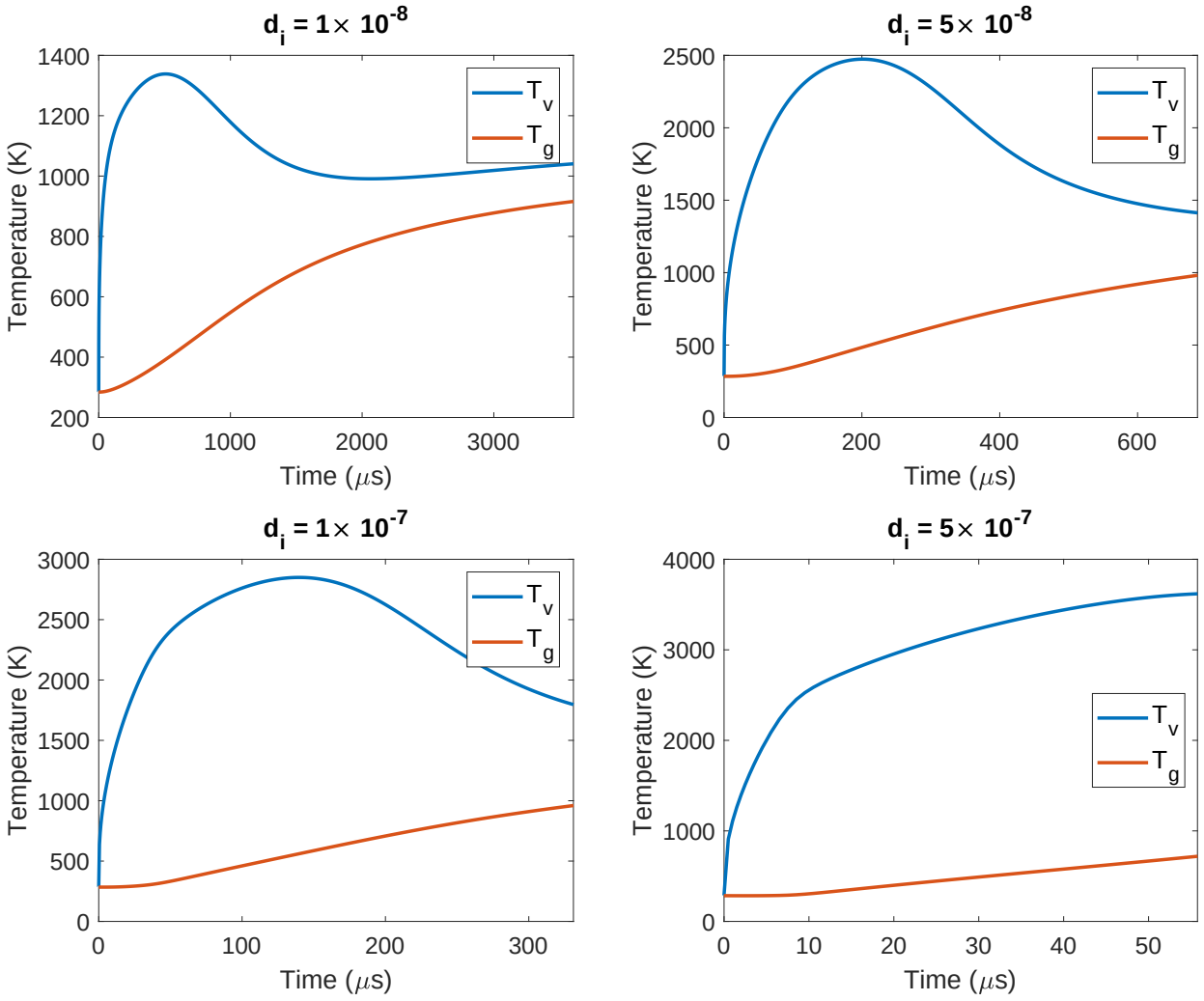

Figure S8: Time-evolution of the vibrational and gas temperature in a continuous plasma for different ionization degrees, and a reduced electric field of 150 Td.

8 Dissociation Mechanisms for Different Reduced Electric Fields and an Ionization Degree of 10^{-7}

In figures 11 and 12 of the main paper, it was shown that at low ionization degrees, plasma pulsing did not enhance the energy efficiency of the continuous plasma, while we showed above that the vibrational temperature did thermalize at the end of the continuous plasma (see e.g. $d_i = 10^{-7}$ in figures S6-S8). In this section, we will explain this by examining the dissociation mechanisms for pulsed plasmas with an ionization degree of 10^{-7}, at reduced electric fields of 50 Td, 100 Td, and 150 Td (figures S9- S11). In figure S9, the conversion by the three main dissociation mechanisms is shown for different plasma pulse times, at an interpulse time of 1 s, a reduced electric field of 50 Td, and an ionization degree of 10^{-7}. The corresponding values for the continuous plasma are indicated with horizontal lines in the same color. At short plasma pulse times, only electron impact dissociation plays a role, and vibrational induced dissociation is negligible. Indeed, the VDF does not have enough time to get fully populated. At plasma pulse times of 200 μs and above, vibrational induced dissociation upon collision with a molecule M shows an increased performance with respect to the continuous plasma, but it is not the most important dissociation process. Indeed, electron impact dissociation is still more important. Nevertheless, the conversion due to electron impact dissociation is severely reduced upon pulsing, as illustrated in figure S9. This reduction is enough to counter the increase in vibrational induced dissociation upon collision with a molecule M, and will therefore lead to a lower total conversion and energy efficiency. Upon increasing reduced electric field, electron impact dissociation becomes more important,[S42] so similar trends are observed in figures S10 and S11 for 100 Td and 150 Td, respectively, again at an ionization degree of 10^{-7}, where also the rise in vibrational induced dissociation is countered by a drop in electron impact dissociation.

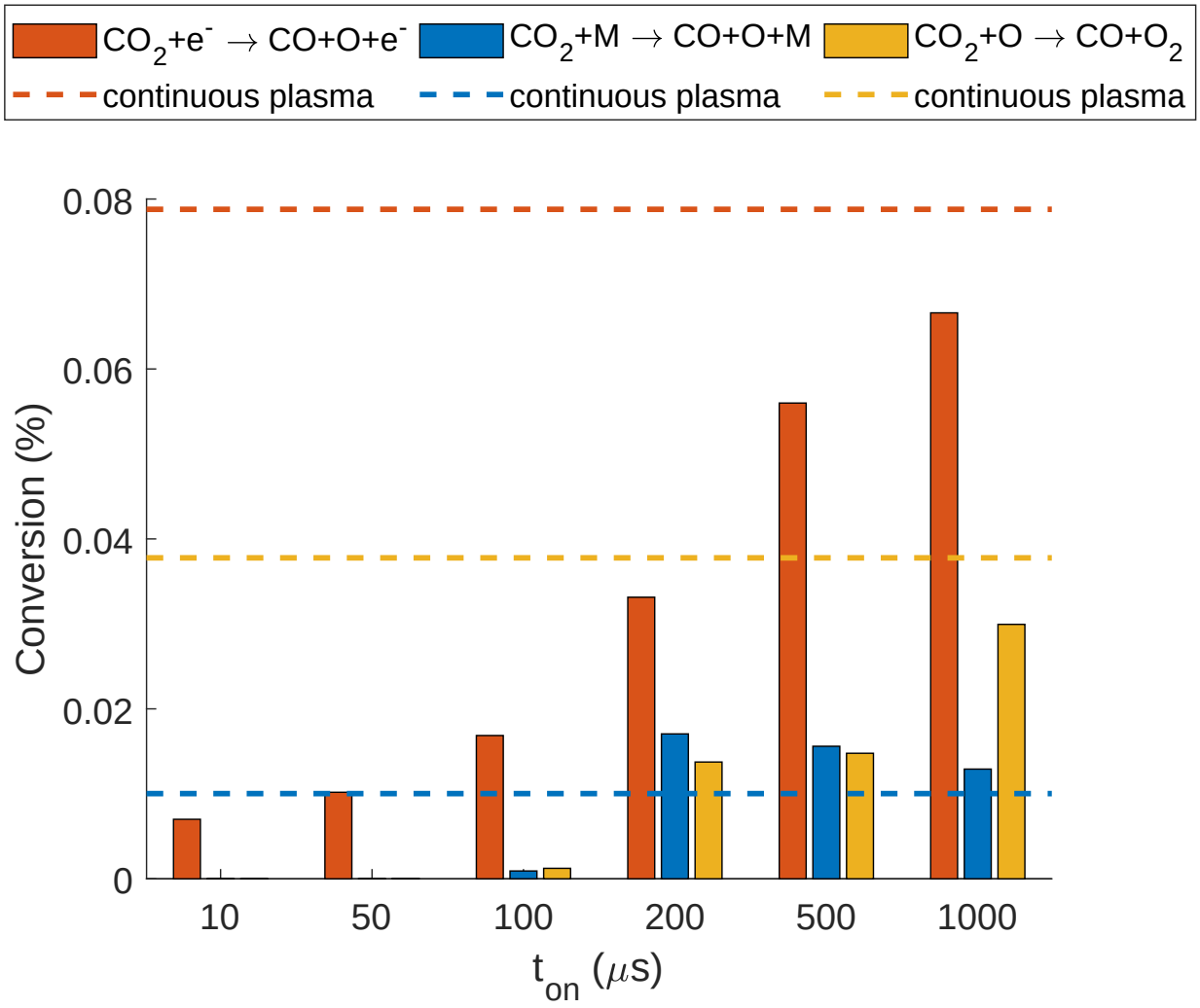

Figure S9: CO_2 conversion by the three main dissociation reactions: electron impact dissociation (red), dissociation upon collision with a molecule M (blue) and upon collision with an O atom (yellow), for different plasma pulse times and an interpulse time of 1 s, a reduced electric field of 50 Td and an ionization degree of 10^{-7}. The dashed horizontal lines represent the respective conversions of a continuous plasma at the same SEI.

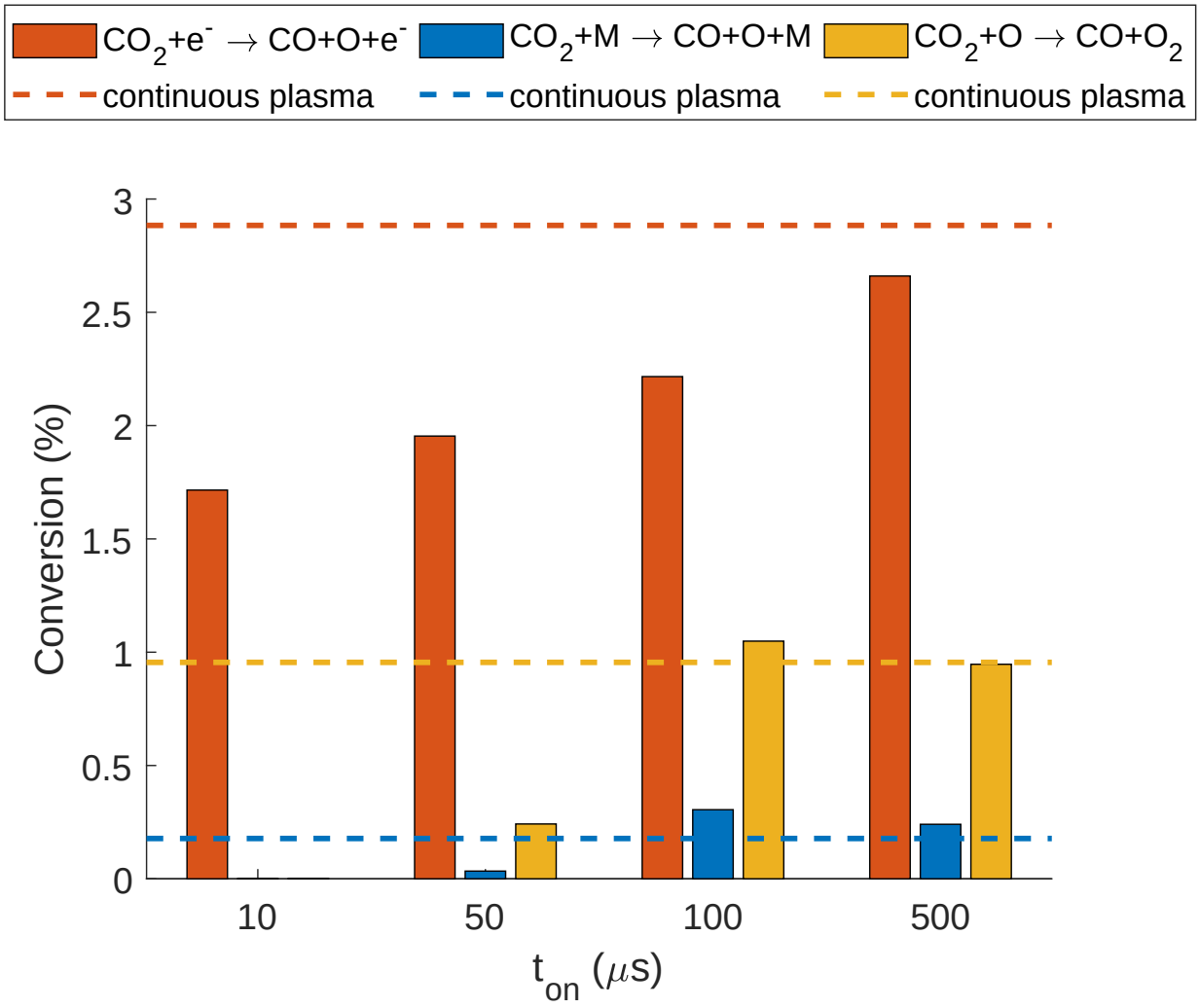

Figure S10: CO_2 conversion by the three main dissociation reactions: electron impact dissociation (red), dissociation upon collision with a molecule M (blue) and upon collision with an O atom (yellow), for different plasma pulse times and an interpulse time of 1 s, a reduced electric field of 100 Td and an ionization degree of 10^{-7}. The dashed horizontal lines represent the respective conversions of a continuous plasma at the same SEI.

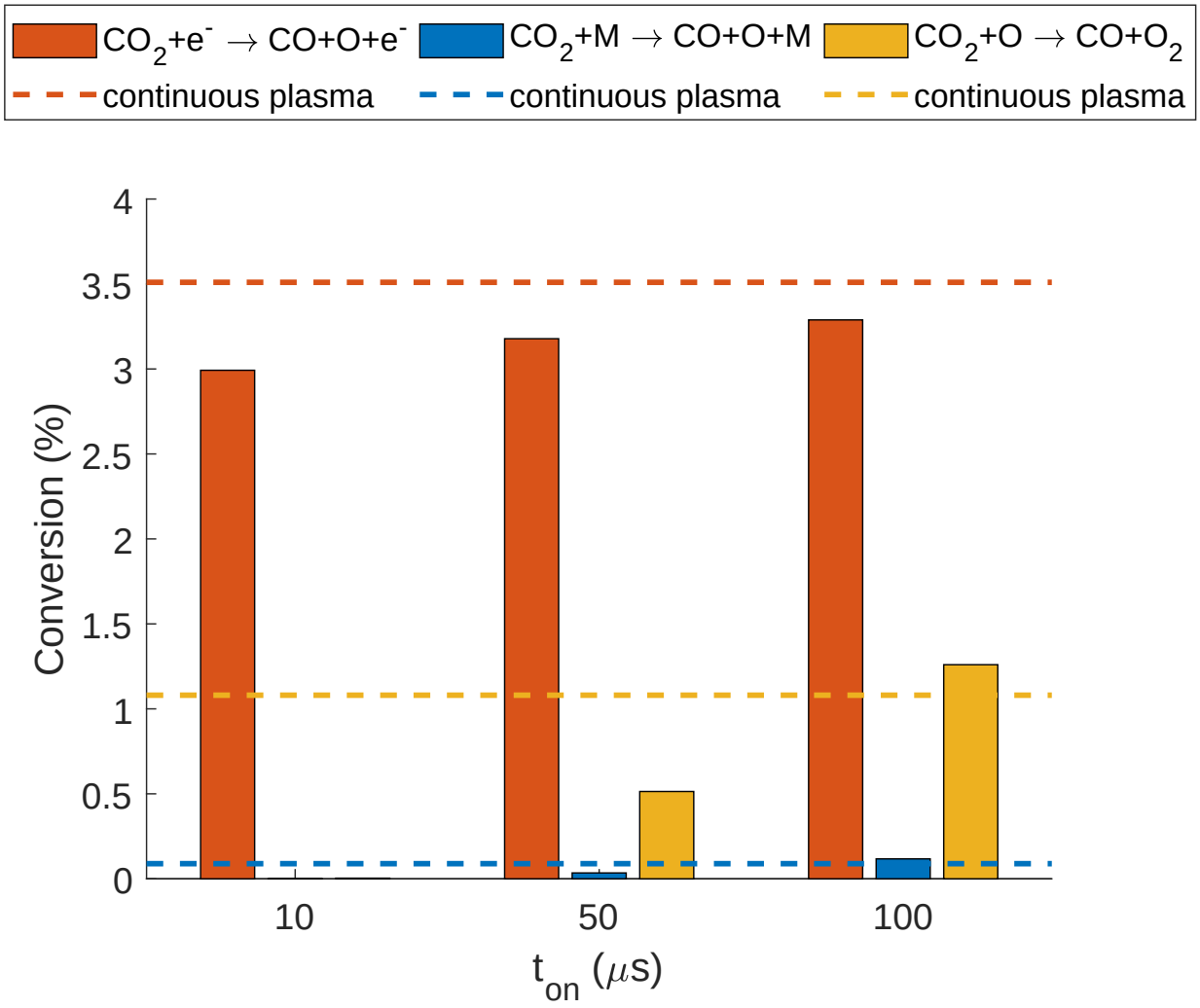

Figure S11: CO_2 conversion by the three main dissociation reactions: electron impact dissociation (red), dissociation upon collision with a molecule M (blue) and upon collision with an O atom (yellow), for different plasma pulse times and an interpulse time of 1 s, a reduced electric field of 150 Td and an ionization degree of 10^{-7}. The dashed horizontal lines represent the respective conversions of a continuous plasma at the same SEI.

9 References

References

(S1) Phelps, A. V. Phelps Database from www.lxcat.net (retrieved September 4, 2014).

(S2) Tian, C.; Vidal, C. R. Cross Sections of the Electron Impact Dissociative Ionization of CO, CH_4 and C_2H_2. *J. Phys. B: At. Mol. Opt. Phys.* **1998**, *31*, 895–909.

(S3) Rapp, D.; Briglia, D. D. Total Cross Sections for Ionization and Attachment in Gases by Electron Impact. II. Negative Ion Formation. *J. Chem. Phys.* **1965**, *43*, 1480–1489.

(S4) Land, J. E. Electron Scattering Cross Sections for Momentum Transfer and Inelastic Excitation in Carbon Monoxide. *J. Appl. Phys.* **1978**, *49*, 5716–5721.

(S5) Lawton, S. A.; Phelps, A. V. Excitation of the $b^1\Sigma_g^+$ State of O_2 by Low Energy Electrons. *J. Chem. Phys.* **1978**, *69*, 1055.

(S6) Weller, C. S.; Biondi, M. A. Measurements of Dissociative Recombination of CO_2^+ Ions with Electrons. *Phys. Rev. Lett.* **1967**, *19*, 59–61.

(S7) Thoenes, J.; Kurzius, S. C. *Plasma Chemistry Processes in the Closed Cycle EDL*; Technical Report DRCPM-HEL-CR-79-11-VOL-1, 1979.

(S8) Beuthe, T. G.; Chang, J.-S. Chemical Kinetic Modelling of Non-Equilibrium Ar-CO_2 Thermal Plasmas. *Jpn. J. Appl. Phys.* **1997**, *36*, 4997–5002.

(S9) Mitchell, J. B. A.; Hus, H. The Dissociative Recombination and Excitation of CO^+. *J. Phys. B: At. Mol. Phys.* **1985**, *18*, 547–555.

(S10) McElroy, D.; Walsh, C.; Markwick, A. J.; Cordiner, M. A.; Smith, K.; Millar, T. J. The UMIST database for astrochemistry 2012. *Astron. Astrophys.* **2013**, *550*, A36.

(S11) Albritton, D. Ion-Neutral Reaction-Rate Constants Measured in Flow Reactors through 1977. *At. Data Nucl. Data Tables* **1978**, *22*, 1–101.

(S12) Adams, N.; Smith, D.; Grief, D. Reactions of H_nCO^+ Ions with Molecules at 300 K. *Int. J. Mass Spectrom. Ion Phys.* **1978**, *26*, 405–415.

(S13) Fehsenfeld, F. C.; Ferguson, E. E. Laboratory Studies of Negative Ion Reactions with Atmospheric Trace Constituents. *J. Chem. Phys.* **1974**, *61*, 3181–3193.

(S14) Mcfarland, M.; Albritton, D. L.; Fehsenfeld, F. C.; Ferguson, E. E.; Schmeltekopf, A. L. Flow-Drift Technique for Ion Mobility and Ion-Molecule Reaction Rate Constant Measurements. III. Negative Ion Reactions of O^- with CO, NO, H_2, and D_2. *J. Chem. Phys.* **1973**, *59*, 6629–6635.

(S15) Price, D.; Moruzzi, J. Negative Ion Molecule Reactions in CO_2 at High Pressures and Temperatures. *Vacuum* **1974**, *24*, 591–593.

(S16) Fehsenfeld, F. C.; Schmeltekopf, A. L.; Schiff, H. I.; Ferguson, E. E. Laboratory Measurements of Negative Ion Reactions of Atmospheric Interest. *Planet. Space Sci.* **1967**, *15*, 373–379.

(S17) Belostotsky, S. G.; Economou, D. J.; Lopaev, D. V.; Rakhimova, T. V. Negative Ion Destruction by $O(^3P)$ Atoms and $O_2(a^1\Delta_g)$ Molecules in an Oxygen Plasma. *Plasma Sources Sci. Technol.* **2005**, *14*, 532–542.

(S18) Pack, J. L.; Phelps, A. V. Electron Attachment and Detachment. II. Mixtures of O_2 and CO_2 and of O_2 and H_2O. *J. Chem. Phys.* **1966**, *45*, 4316–4329.

(S19) Bortner, M. H.; Bourer, T.; Blank, C. A. *Defense Nuclear Agency Reaction Rate Handbook, Second Edition*; Technical report AD 763699, 1972.

(S20) Hasted, J. B.; Smith, R. A. The Detachment of Electrons from Negative Ions. *Proc. R. Soc. London, Ser. A* **1956**, *235*, 349–353.

(S21) Frommhold, L. Über Verzögerte Elektronen in Elektronenlawinen, insbesondere in Sauerstoff und Luft, durch Bildung und Zerfall Negativer Ionen (O^-). *Fortschr. Phys.* **1964**, *12*, 597–642.

(S22) Gudmundsson, J. T. *A Critical Review of the Reaction set for a Low Pressure Oxygen Processing Discharge*; Technical Report RH-17-2004, 2004.

(S23) Fridman, A. *Plasma Chemistry*; Cambridge University Press: New York, USA, 2008.

(S24) Kozák, T.; Bogaerts, A. Splitting of CO_2 by Vibrational Excitation in Non-Equilibrium Plasmas: a Reaction Kinetics Model. *Plasma Sources Sci. Technol.* **2014**, *23*, 045004.

(S25) Burmeister, M.; Roth, P. ARAS Measurements on the Thermal Decomposition of CO_2 Behind Shock Waves. *AIAA Journal* **1990**, *28*, 402–405.

(S26) Clark, T. C.; Garnett, S. H.; Kistiakowsky, G. B. Reaction of Carbon Dioxide with Atomic Oxygen and the Dissociation of Carbon Dioxide in Shock Waves. *J. Chem. Phys.* **1969**, *51*, 2885–2891.

(S27) Husain, D.; Young, A. N. Kinetic Investigation of Ground State Carbon Atoms, $C(2^3P_J)$. *J. Chem. Soc., Faraday Trans. 2* **1975**, *71*, 525.

(S28) Baldwin, R. R.; Jackson, D.; Melvin, A.; Rossiter, B. N. The Second Limit of Hydrogen + Carbon Monoxide + Oxygen Mixtures. *Int. J. Chem. Kinet.* **1972**, *4*, 277–292.

(S29) Tsang, W.; Hampson, R. F. Chemical Kinetic Data Base for Combustion Chemistry. Part I. Methane and Related Compounds. *J. Phys. Chem. Ref. Data* **1986**, *15*, 1087–1279.

(S30) Dean, A. J.; Davidson, D. F.; Hanson, R. K. A Shock Tube Study of Reactions of Carbon Atoms with Hydrogen and Oxygen using Excimer Photolysis of C_3O_2 and

Carbon Atom Atomic Resonance Absorption Spectroscopy. *J. Phys. Chem.* **1991**, *95*, 183–191.

(S31) Baulch, D. L.; Drysdale, D. D.; Duxbury, J.; Grant, S. *Evaluated Kinetic Data for High Temperature Reactions, Volume 3: Homogeneous Gas Phase Reactions of the O_2-O_3 System, the CO-O_2-H_2 System, and of the Sulphur-containing Species*; Butterworth: London, UK, 1976.

(S32) Simpson, C. J. S. M.; Chandler, T. R. D.; Strawson, A. C. Vibrational Relaxation in CO_2 and CO_2–Ar Mixtures Studied Using a Shock Tube and a Laser–Schlieren Technique. *J. Chem. Phys.* **1969**, *51*, 2214–2219.

(S33) Taylor, R. L.; Bitterman, S. Survey of Vibrational Relaxation Data for Processes Important in the CO_2-N_2 Laser System. *Rev. Mod. Phys.* **1969**, *41*, 26–47.

(S34) Blauer, J. A.; Gilmore, G. R. *A Survey of Vibrational Relaxation Rate Data for Processes Important to CO_2-N_2-H_2O Infrared Plume Radiation*; Technical Report AFRPL-TR-73-57, 1973.

(S35) Rosser, W. A.; Wood, A. D.; Gerry, E. T. Deactivation of Vibrationally Excited Carbon Dioxide (ν_3) by Collisions with Carbon Dioxide or with Nitrogen. *J. Chem. Phys.* **1969**, *50*, 4996–5008.

(S36) Herzfeld, K. F. Deactivation of Vibrations by Collision in the Presence of Fermi Resonance. *J. Chem. Phys.* **1967**, *47*, 743–752.

(S37) Capitelli, M.; Ferreira, C. M.; Gordiets, B. F.; Osipov, A. I. *Plasma Kinetics in Atmospheric Gases*; Springer Berlin Heidelberg: Berlin, Germany, 2000.

(S38) Sharma, R. D. Near Resonant Vibrational Energy Transfer among Isotopes of CO_2. *Phys. Rev.* **1969**, *177*, 102–107.

(S39) Kreutz, T. G.; O'Neill, J. A.; Flynn, G. W. Diode Laser Absorption Probe of Vibration-Vibration Energy Transfer in CO_2. *J. Phys. Chem.* **1987**, *91*, 5540–5543.

(S40) DeLeon, R. L.; Rich, J. Vibrational Energy Exchange Rates in Carbon Monoxide. *Chem. Phys.* **1986**, *107*, 283–292.

(S41) Flament, C.; George, T.; Meister, K.; Tufts, J.; Rich, J.; Subramaniam, V.; Martin, J.-P.; Piar, B.; Perrin, M.-Y. Nonequilibrium Vibrational Kinetics of Carbon Monoxide at high Translational Mode Temperatures. *Chem. Phys.* **1992**, *163*, 241–262.

(S42) Berthelot, A.; Bogaerts, A. Pinpointing Energy Losses in CO_2 Plasmas - Effect on CO_2 Conversion. *J. CO_2 Util.* **2018**, *24*, 479–499.